



HAL
open science

When RNA meets montmorillonite: Influence of the pH and divalent cations

Luís de Oliveira, Pollyana Trigueiro, Baptiste Rigaud, Edson da Silva-Filho, Josy Osajima, Maria Fonseca, Jean-François Lambert, Thomas Georgelin, Maguy Jaber

► To cite this version:

Luís de Oliveira, Pollyana Trigueiro, Baptiste Rigaud, Edson da Silva-Filho, Josy Osajima, et al.. When RNA meets montmorillonite: Influence of the pH and divalent cations. *Applied Clay Science*, 2021, 214, pp.106234. 10.1016/j.clay.2021.106234 . hal-03990019

HAL Id: hal-03990019

<https://hal.science/hal-03990019>

Submitted on 16 Oct 2023

HAL is a multi-disciplinary open access archive for the deposit and dissemination of scientific research documents, whether they are published or not. The documents may come from teaching and research institutions in France or abroad, or from public or private research centers.

L'archive ouverte pluridisciplinaire **HAL**, est destinée au dépôt et à la diffusion de documents scientifiques de niveau recherche, publiés ou non, émanant des établissements d'enseignement et de recherche français ou étrangers, des laboratoires publics ou privés.



Distributed under a Creative Commons Attribution - NonCommercial 4.0 International License

33

34

35 **Introduction**

36 Interactions between biomolecules and clay minerals are key for different fields like
37 separations processes and hybrid nanomaterials. Among clay minerals, montmorillonites
38 belong to the group of smectites with a 2:1 layer structure, negative surface charges (due to
39 isomorphic substitutions), counterbalanced by cations present in the interlayer space, high
40 internal surface area, cation exchange capacity and reactive groups on their surfaces, as well
41 as the ability to confine molecules in the interlayer space (Jaber and Miehé-Brendlé, 2008;
42 Wu et al., 2015; Escamilla-Roa et al., 2017). These intrinsic properties make them possible
43 "hosts" for biomolecules such as RNA (James Cleaves et al., 2012; Ruiz-Mirazo et al., 2014).

44 The mechanisms of nitrogen bases, nucleotides and RNA/montmorillonite interactions
45 have been reviewed and both electrostatic interactions and hydrogen bonding were found to
46 play a role (Yu et al., 2013). Some studies suggested the participation of the interlayer cations
47 as a "bridge" for interaction between the negatively charged clay surface and the phosphate of
48 the RNA, which also bears a negative charge (Franchi et al., 2003; Pedreira-Segade et al.,
49 2018; Hao et al., 2019). Alkaline earth metal cations have been observed to strongly enhance
50 the adsorption of single-strand (but not double-strand) RNA to montmorillonite (Gujjari et al.,
51 2018). Some studies suggest the likely presence of these metallic cations in rocks and in the
52 primitive ocean (Eder and Rode, 1994; Izawa et al., 2010). They are important for the folding,
53 structure and function of RNA, especially the divalent ion Mg^{2+} (Pyle, 2002; Leonarski et al.,
54 2017), and their involvement has been suggested in the stabilization and/or activation of
55 biological macromolecules (Black et al., 1994). Villafañe-Barajas et al. have also underlined
56 the importance of added cations for the adsorption of nucleotides, the monomers of RNA; and

57 molecular modelling studies (Carrascoza et al., 2019) suggest that they could play a
58 significant role in the reactivity of adsorbed organic molecules.

59

60 pH is a key parameter that controls the adsorption of biomolecules, since acido-basic
61 speciation determines the electrostatic interaction between RNA and the surface (Theng et al.,
62 1982; Lawless et al., 1985). Some studies in recent years have addressed the interaction of
63 nitrogen bases (Benetoli et al., 2008; Hashizume et al., 2010; Carneiro et al., 2011),
64 nucleotides (Feuillie et al., 2013; Pedreira-Segade et al., 2016; Hao et al., 2019) and less often
65 nucleosides (Fornaro et al., 2018) with montmorillonite, varying the pH and the nature of
66 metal cations, and trying to elucidate the types of interactions between these molecules and
67 montmorillonite. However, the interactions of polymeric RNA with the surface of clay
68 minerals remain understudied, especially at the molecular level. In this perspective, the aim of
69 this study was to evaluate the adsorption of RNA (ribonucleic acid diethylaminoethanol salt)
70 on montmorillonite in order to contribute to the understanding of a bigger puzzle, the origin of
71 life. The organic-inorganic interactions were investigated at the molecular level and the
72 influence of different parameters such as nature of the interlayer cation (Na^+ , Ca^{2+} , Mg^{2+} , and
73 Sr^{2+}) and the pH was evaluated.

74 **2. Materials and Methods**

75 **2.1. Chemicals**

76 Ribonucleic acid diethylaminoethanol salt (diethylethanolammonium; ribonucleic acid
77 derived from Torula yeast, CAS 63231-63-0, Sigma-Aldrich), hydrofluoric acid (HF, 40%
78 w/w, Fluka), sodium acetate (CH_3COONa , 99%, Sigma-Aldrich), magnesium acetate
79 ($(\text{CH}_3\text{COO})_2\text{Mg} \cdot 4\text{H}_2\text{O}$, 99%, Sigma-Aldrich), Al_2O_3 (98%, Pural-Sasol), and SiO_2 (99.8%,

80 Aerosil 130, Evonik Industries). The others chemicals were purchased from Sigma-Aldrich
81 (analytical grade). All chemicals were used without any previous purification.

82 **2.2. Synthesis of montmorillonite**

83 The sodium montmorillonite (Na-Mt) used in this work was synthesized according to
84 the procedure described previously (Jaber and Miehé-Brendlé, 2005; Jaber and Miehé-
85 Brendlé, 2008; Trigueiro et al., 2018b, 2018a) and had the ideal formula per half unit cell
86 $\text{Na}_{0.2}[\text{Si}_4\text{Al}_{1.8}\text{Mg}_{0.2}\text{O}_{10}(\text{OH},\text{F})_2]$. The reagents were mixed in the following order: 196.860 g of
87 deionized water, 2.410 g of hydrofluoric acid, 0.990 g of sodium acetate, 2.587 g of
88 magnesium acetate, 3.325 g of alumina and 7.249 g of silica. The obtained hydrogel was aged
89 under stirring at room temperature for 2 h and then was autoclaved at 220°C for 72 h. The
90 autoclave was cooled to room temperature and the product was thoroughly washed with
91 distilled water and centrifuged. Finally, the synthesized Na-Mt was dried at 50°C for 72 h.
92 The synthesis conditions had previously been optimized for the crystallization of pure
93 montmorillonite. The Al/Mg ratio influenced the preferential location of Al^{3+} in the
94 tetrahedral sheets. The initial pH of the hydrogel, around 5, determined the di- or tri-
95 octahedral character of the obtained phyllosilicate and the Si/F ratio as well as the synthesis
96 time influenced the crystallinity of pure montmorillonite (Reinholdt et al., 2001, 2005).

97 **2.3. Ion exchange reaction**

98 The ion exchange of Na-Mt was performed according to previously published
99 procedures (Lepoitevin et al., 2014). Na-Mt was suspended in 1 mol L⁻¹ of $\text{CaCl}_2 \cdot 2\text{H}_2\text{O}$,
100 $\text{MgCl}_2 \cdot 6\text{H}_2\text{O}$ or $\text{Sr}(\text{NO}_3)_2$ solutions for 24 h under magnetic stirring at 25°C. Then, the
101 obtained materials were centrifuged, washed in deionized water and dried at 50°C. The same
102 process was repeated twice. Finally, the solids were washed and dried in the same conditions.
103 The exchanged montmorillonites will be designated as Ca-Mt, Mg-Mt, and Sr-Mt.

104 **2.4. Adsorption of RNA salt on montmorillonite**

105 The adsorption of RNA on the exchanged montmorillonites was performed according
106 to a procedure published previously (Greaves and Wilson, 1969) with some modifications.
107 Initially, the clay mineral samples (Na-Mt, Ca-Mt, Mg-Mt and Sr-Mt) were dispersed in water
108 at a 1.25 mg mL^{-1} concentration over a period of 4 h under magnetic stirring at 25°C . In all
109 cases, the natural pH of all clay mineral dispersions was around 5.0. Then, 1 mg mL^{-1} of RNA
110 solution (pH 6.8) was slowly added. The RNA/Mt ratio was 2:1 w/w for all systems. After
111 this step, the pH of all systems was between 6.2-6.5 without pH adjustment. The system was
112 kept under magnetic stirring for 16 h at 25°C . The same procedure was also performed for all
113 systems at pH 2.9-3.1, adjusted with 0.5 mol L^{-1} of the HCl solution. The resulting samples
114 were centrifuged, washed with deionized water and dried at 50°C overnight. As a control, Na-
115 Mt was maintained at pH 3.0 without RNA in the same conditions and analyzed after the
116 reaction.

117 **2.5. Characterizations**

118 **X-ray diffraction (XRD):** powder X-ray diffraction was carried out on a Shimadzu
119 XRD-6000 model diffractometer equipped with a monochromatic $\text{CuK}\alpha$ ($\lambda = 0.15406 \text{ nm}$)
120 source operating at 2 kVA, 40 kV, and 30 mA. The diffraction patterns were recorded from 3
121 to 80° with a scan rate of $0.5^{\circ} \text{ min}^{-1}$ in the same conditions as for previous works (França et
122 al., 2020; da Silva et al., 2021).

123 **Scanning electron microscopy (SEM):** Scanning electron microscopy was performed
124 using a FEI/Thermo Fischer, model Quanta FEG 250 with cannon per field and an
125 acceleration voltage of 1 to 30 kV. Samples were fixed on carbon tape and coated with gold in
126 a Quorum model Q150R sputter-coater for 35 s at 20 mA by a plasma generated under an
127 argon atmosphere.

128 **Fourier transform infrared spectroscopy:** the FTIR spectra of samples - dispersed
129 in KBr pellets containing approximately 1% (w/w) of the sample - were recorded using a
130 Shimadzu PESTIGE – 21 model spectrometer over the 4000 – 400 cm⁻¹ range at a resolution
131 of 4 cm⁻¹ and with 30 scans for each run.

132 **Thermal analyses (TG-DTG):** Thermogravimetric analyses and derivate
133 thermogravimetry were performed using equipment from TA Instruments SDT Q600 model.
134 The samples were heated from 20 to 1000°C in an alumina crucible with a heating rate of
135 10°C min⁻¹ under nitrogen flow.

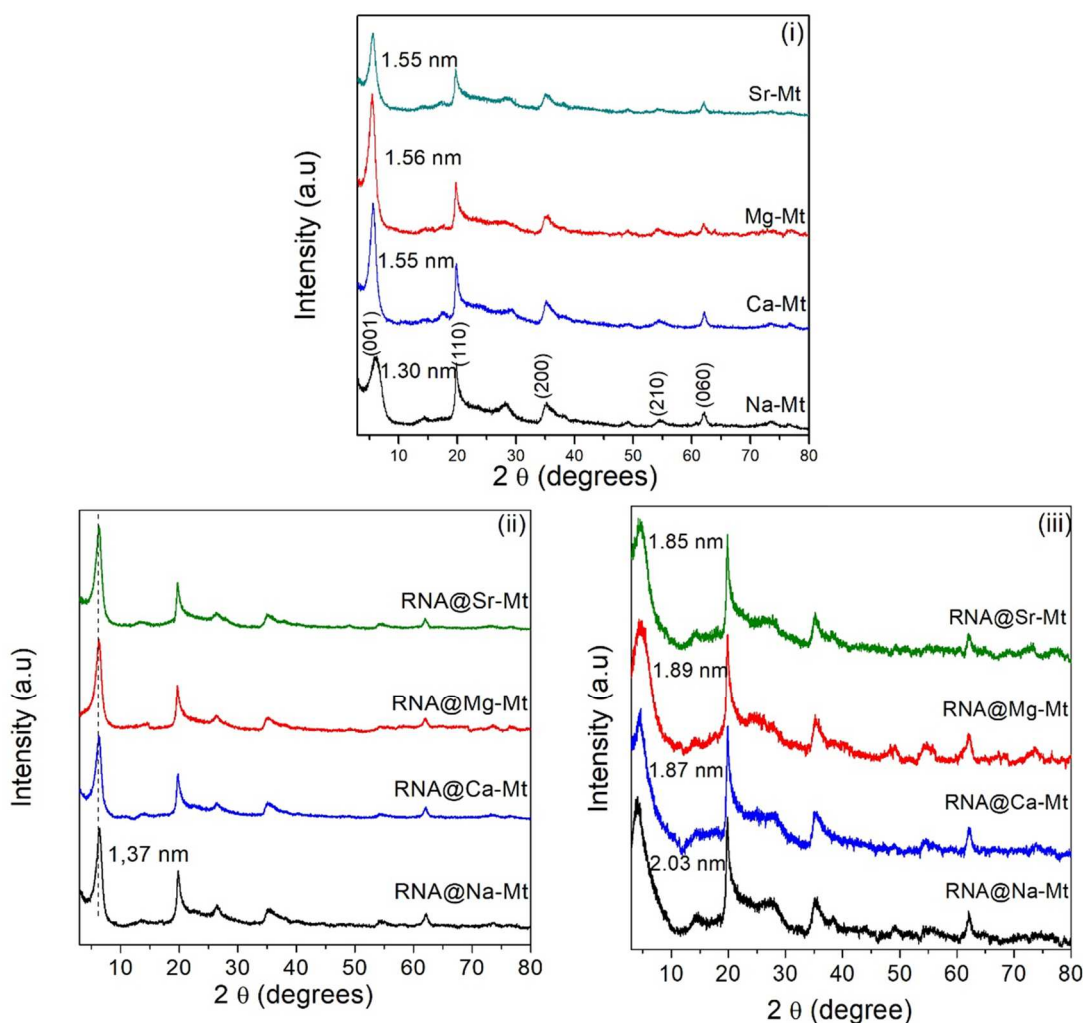
136 **Solid state nuclear magnetic resonance:** ³¹P, ¹³C, and ²⁷Al MAS NMR spectra were
137 obtained on a Bruker Avance III spectrometer equipped with a 4 mm H-X probe, operating at
138 Larmor frequencies of 500.17 MHz (¹H), 202.47 MHz (³¹P), 125.77 MHz (¹³C) and 130.33
139 MHz (²⁷Al) based on previous studies (Guillermin et al., 2019; Rodrigues et al., 2019;
140 Cavalcanti et al., 2021). Chemical shifts were calibrated using triphenylphosphine (19.64
141 ppm) for ³¹P, the carboxyl signal of adamantane (38.52 ppm) for ¹³C, and AlNO₃ (0 ppm) for
142 ²⁷Al as external standards. All spectra were recorded with a spinning rate of 14 kHz. The ¹³C
143 Cross-Polarization spectra were acquired with a ramp-CP contact time of 2 ms and a 1.5 s
144 recycle delay and with a ¹H decoupling spinal 64. The acquisition time was 40 ms. The
145 number of scans to obtain the spectra varied depending on the S/N obtained for each sample.
146 Spectra were processed with a zero-filling factor of 2 and with an exponential decay
147 corresponding to a 50 Hz line broadening in the transformed spectra. Only spectra with the
148 same line broadening are directly compared. ²⁷Al single-pulse spectra using a 30° pulse were
149 recorded with 100 kHz spectral width and with a recycle delay of 500. ³¹P experiments using
150 a 90° pulse were acquired with a recycle delay of 5 s and with a ¹H decoupling spinal 64.

151 **3. Results**

152 **3.1. XRD diffraction**

153 XRD patterns of the sodium and exchanged montmorillonites and resulting RNA-Mt
154 hybrids are presented in Figure 1. A reflection at 6.77° (2θ), corresponding to a d_{001} -value of
155 1.30 nm, was observed for Na-Mt. Other reflections were observed at $2\theta = 19.91^\circ$, 35.31° ,
156 54.71° and 62.13° and were indexed to (110) (0.445 nm), (200) (0.253 nm), (210) (0.167 nm)
157 and (060) (0.149 nm) reticular planes, respectively (Jaber et al., 2014; Trigueiro et al., 2018a).
158 The formation of the Na-Mt was monitored by SEM (Figure SM-1). Well-formed particles in
159 typical plates morphology were observed without the presence of other phases.

160 For all ion-exchanged samples, the (001) reflections shifted up to 1.56 nm.



161

162 **Figure 1:** XRD patterns of (i) Na-Mt, Ca-Mt, Mg-Mt, and Sr-Mt montmorillonites and of the
 163 RNA@cations-Mt hybrids prepared at (ii) pH 6.2-6.5 and (iii) pH 2.9-3.1.

164

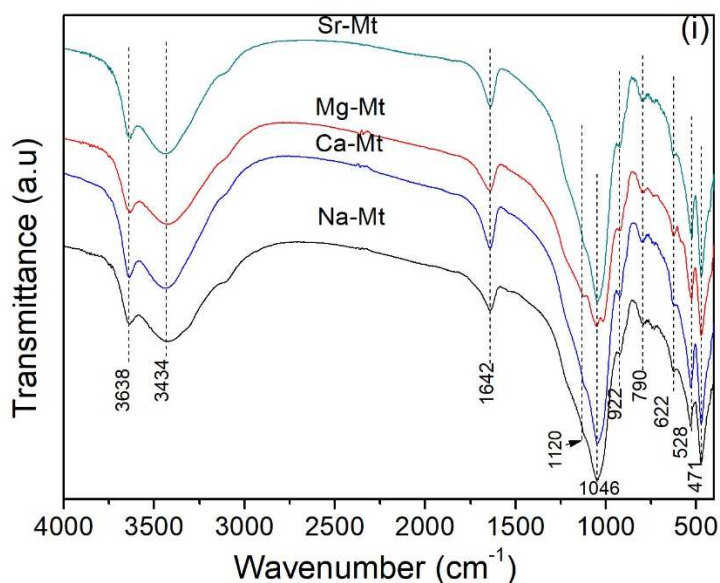
165 After adsorption, the observed pH of the solutions varied between 6.2-6.5 and 2.9-3.1,
 166 for systems without and with pH adjustment. Figure 1(ii) depicts the XRD patterns of
 167 RNA@cations-Mt at pH 6.2-6.5 and 1(iii) pH 2.9-3.1. At pH 6.2-6.5, the d_{001} -value is 1.37
 168 nm for all samples. At pH 2.9-3.1, in Figure 1(iii), the (001) reflection shifted to higher basal
 169 distances: d_{001} -value= 2.03 nm, 1.87 nm, 1.89 nm, and 1.85 nm in RNA@Na-Mt, RNA@Ca-
 170 Mt, RNA@Mg-Mt and RNA@Sr-Mt, respectively, corresponding to interlayer spacings in
 171 the 0.9 nm range. In contrast, XRD (Figure SM-2) of the Na-Mt maintained in an acidic

172 medium (pH 3) without the presence of RNA molecules presented the same reflections as the
173 original sample. In particular, the d_{001} value stayed at 1.30 nm and did not show any
174 broadening, suggesting that no alteration in long-range order or formation of exfoliated phase
175 occurred in the conditions of the synthesis.

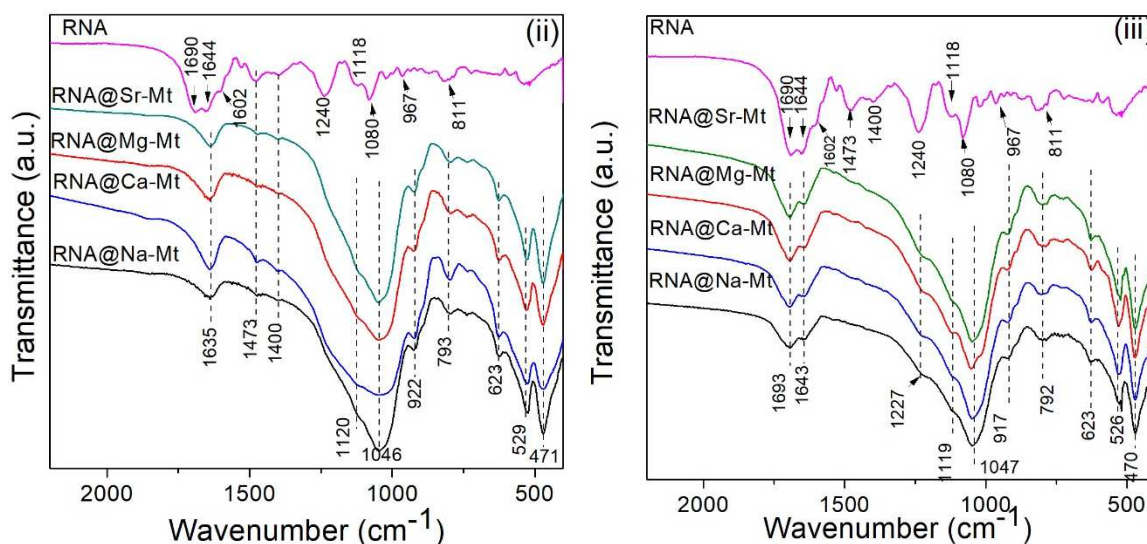
176 **3.2. Infrared spectroscopy**

177 FTIR spectra of the solids before and after RNA adsorption are presented in Figure 2.
178 Irrespective of the compensating cation, the spectra were similar with absorptions at 3638 cm^{-1}
179 and 3400 cm^{-1} (broad) assigned to OH stretching of structural OH and water, respectively
180 (Bizovská et al., 2018). Bands at 1640 and 922 cm^{-1} were attributed to water deformation, and
181 to the OH bending bands in Al_2OH , respectively (Madejová et al., 2017).

182 Absorptions at 1120 cm^{-1} and 1046 cm^{-1} were assigned to Si-O-Si asymmetric and
183 symmetric stretchings, respectively, in the silicate matrix (Bizovská et al., 2018). Two bands
184 at 790 cm^{-1} and 622 cm^{-1} were associated with Al-O-Si bending and to Al-O out-of-plane and
185 Si-O vibrations (Madejová et al., 2017). Furthermore, Al-O-Si and Si-O-Si bending modes
186 were observed at 528 and 471 cm^{-1} , respectively (Pentrák et al., 2018). If amorphous silica
187 was present, it would be detected by absorption bands at 800 - 810 cm^{-1} (Costa et al., 1997;
188 Pentrák et al., 2012; Santos et al., 2015); they were not observed in present case.



189



190

191 **Figure 2.** FTIR spectra for (i) Na-Mt, Ca-Mt, Mg-Mt and Sr-Mt montmorillonites, and
 192 spectra in range 2200 – 400 cm^{-1} for RNA and RNA@cations-Mt hybrids obtained at (ii) pH
 193 6.2-6.5 and (iii) pH 2.9-3.1.

194

195 Figure 2ii and iii shows FTIR spectra in the 400-2000 cm^{-1} range of RNA and solids
 196 after RNA adsorption. FTIR spectra in the complete 400-4000 cm^{-1} range are presented in
 197 Figures SM-2i and ii. The spectrum of RNA presents a band at 3387 cm^{-1} (Figure SM-2i and
 198 ii) associated with the N-H stretch and one at 2954 cm^{-1} due to the C-H stretch (Tsuboi,
 199 1970). The bands at 1690, 1644 and 1602 cm^{-1} were associated with the C=O vibration on

200 purine and pyrimidines (Tsuboi, 1970; Banyay et al., 2003). The absorption band at 1473 cm^{-1}
201 has been attributed to ring vibrations of the uracil base (Kumar and Singh, 2013) and the one
202 at 1400 cm^{-1} was attributed to in-plane C-O-H deformation mode, at 2' in the ribose ring
203 (Tsuboi, 1970; Banyay et al., 2003). The bands at 1240 and 1080 cm^{-1} were attributed to
204 asymmetrical and symmetrical PO_2^- stretch, respectively (Tsuboi, 1970; Benedetti et al., 1997)
205 and the band at 1118 cm^{-1} to the C-O stretch in ribose (Benedetti et al., 1997). Finally, the
206 band at 967 cm^{-1} is an unidentified ribose-phosphate main chain vibrations, and that at 811
207 cm^{-1} is a sugar marker of complex origin (Tsuboi, 1970; Banyay et al., 2003).

208 The spectra of the solids after RNA adsorption in the $400\text{-}2000\text{ cm}^{-1}$ range are
209 depicted in Figures 2ii and iii. At pH 6.2-6.5 (Figure 2ii), similar new bands were observed in
210 the FTIR spectra of the solids, both at the same position as in the spectra of RNA: 1473 cm^{-1}
211 (ring vibrations) and 1400 cm^{-1} (in-plane C-O-H deformation of ribose). Other diagnostic
212 bands of RNA may be present as shoulders, but are hidden by the strong absorption of the
213 clay mineral lattice in the $900\text{-}1200\text{ cm}^{-1}$ region.

214 Infrared spectra of the hybrids obtained in an acidic medium (Figure 2iii) showed
215 different additional bands at 1693 cm^{-1} (C=O stretching in nucleobases). The band of PO_2^- ,
216 observed at 1240 cm^{-1} in RNA spectra (Figure 3), shifted to 1227 cm^{-1} in the RNA@cations-
217 Mt.

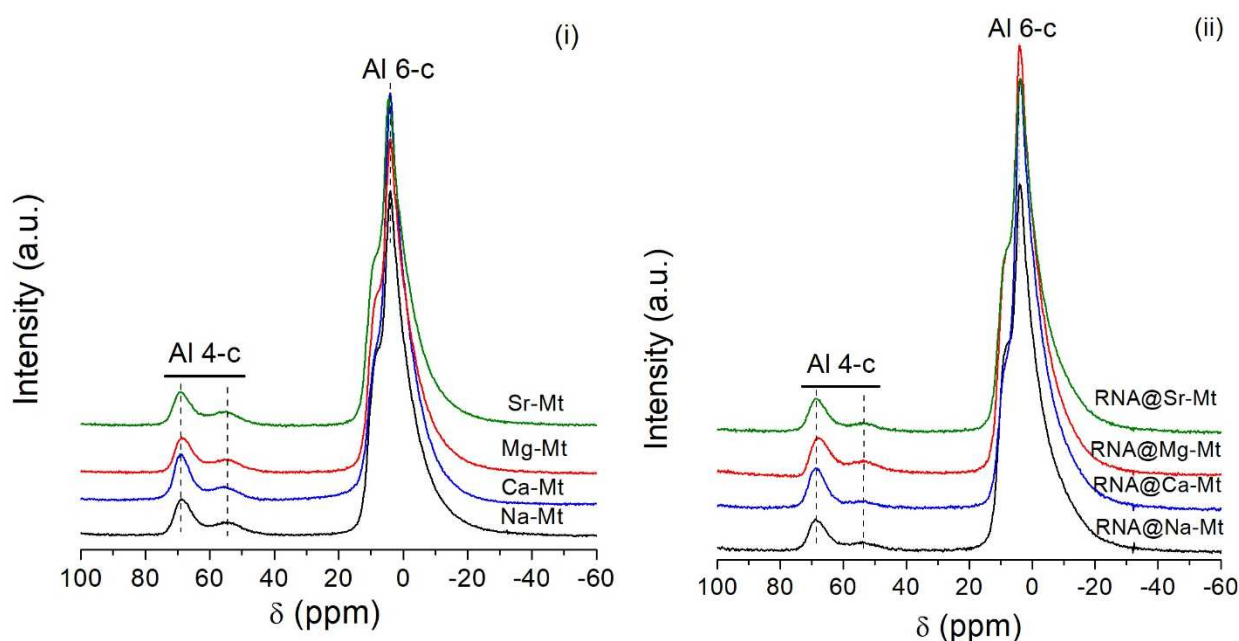
218 Bathochromic shifts of the bands attributed to the structural OH of the clay mineral
219 lattice (cations-Mt: 3638 cm^{-1} , RNA@cations-Mt at pH 6.2-6.5: 3632 cm^{-1} and
220 RNA@cations-Mt at pH 2.9-3.1: 3630 cm^{-1}), were observed (see Supplementary materials
221 Fig. SM-3i and ii).

222 **3.3. ^{27}Al , ^{13}C and ^{31}P solid state NMR**

223 ^{27}Al NMR spectra for samples before and after adsorption of the biomolecule at pH
224 2.9-3.1 are shown in Figure 3i and ii. All precursor samples presented characteristic chemical
225 shifts at 3.9 and 69.1 ppm. Another chemical shift was observed in both spectra at 55 ppm.
226 The same chemical shifts were observed in the RNA@cations-Mt samples.

227

228

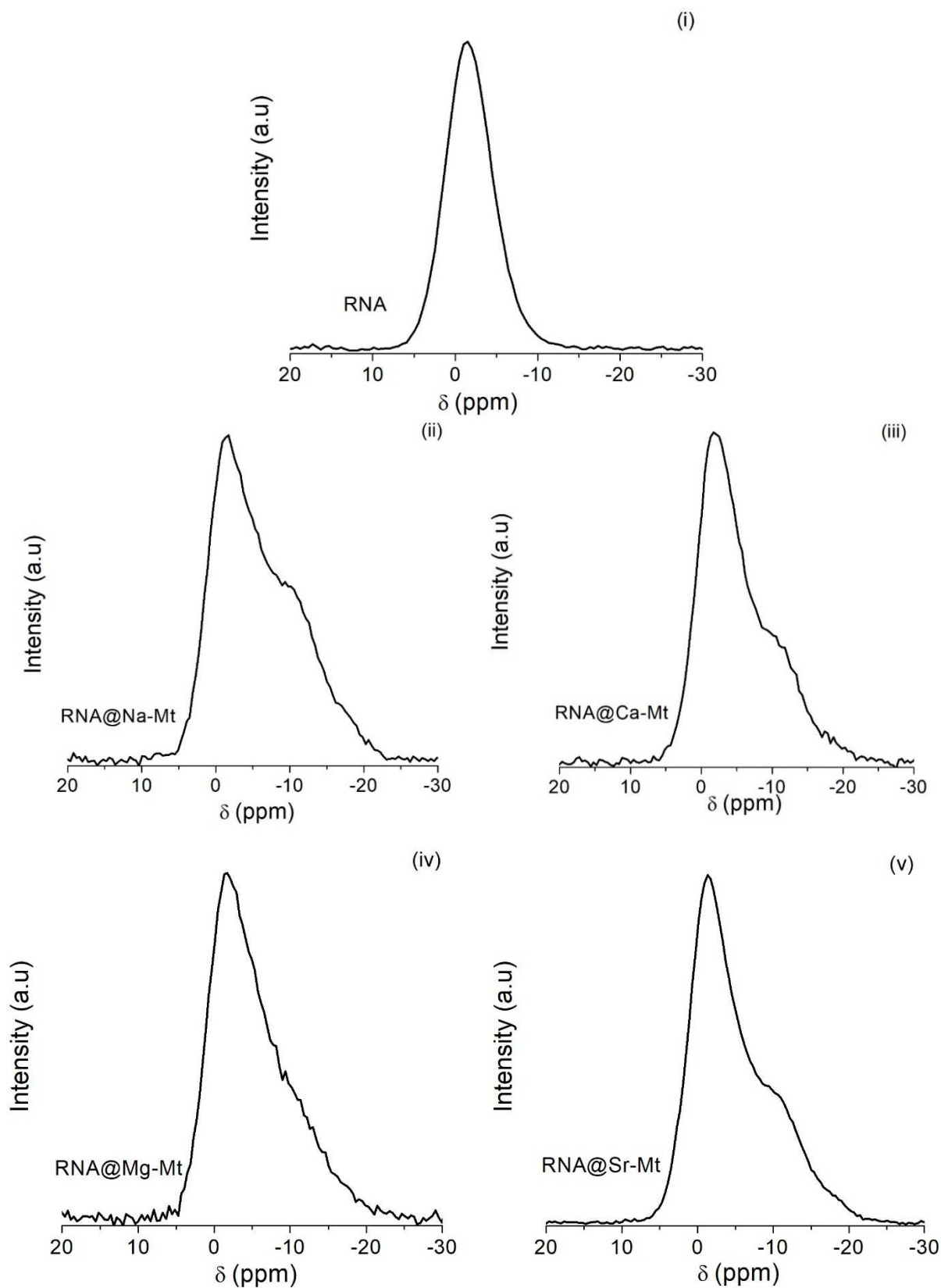


229 **Figure 3.** ^{27}Al NMR spectra of the (i) exchanged montmorillonites and (ii) RNA@Mt hybrids
230 obtained at pH 2.9-3.1.

231

232 The ^{31}P spectrum of RNA is shown in Figure 4i. A broad, asymmetric signal is
233 observed with a maximum at +1.4 ppm. For the RNA@cations-Mt samples, a strong new
234 component appeared at -9.3 to -10.6 ppm, i.e., 8 to 9 ppm upfield from the signal in pristine
235 RNA.

236

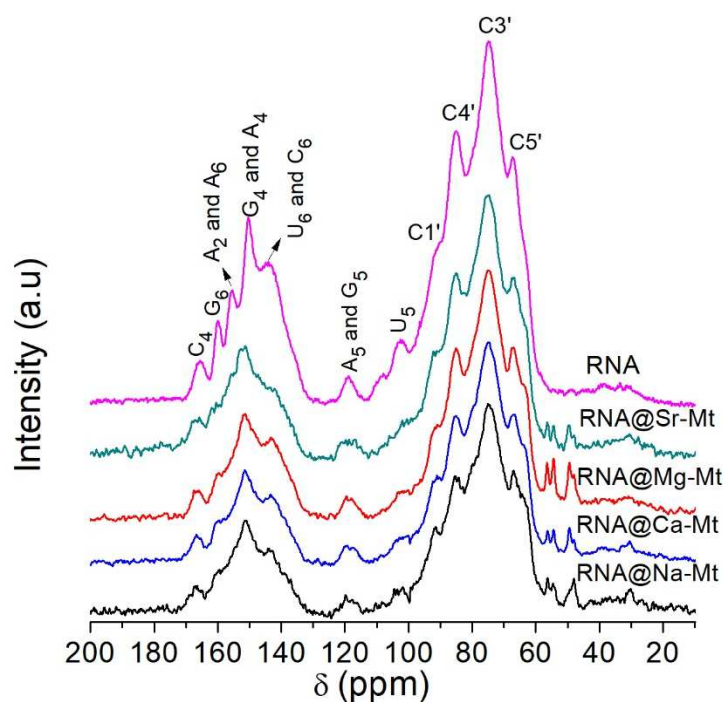


237 **Figure 4.** ^{31}P NMR spectra of RNA (i) and hybrids RNA@Na-Mt (ii), RNA@Ca-Mt (iii),
 238 RNA@Mg-Mt (iv) and RNA@Sr-Mt (v) in pH 2.9-3.1.

239

240 ^{13}C NMR spectra of the RNA and the hybrids obtained at pH 2.9-3.1 are depicted in
241 Figure 5 and values of chemical shifts and respective attributions are summarized in Table 1.
242 The observed NMR signals for the RNA@Mt hybrids were similar.

243 The signals at 60 – 90 ppm were assigned to carbons in the ribose moiety (Chang et
244 al., 1982; Rodrigues et al., 2019). Signals in the 100 - 170 ppm range were attributed to the
245 nucleotides bases (Chang et al., 1982; Fujiwara et al., 1995). In particular, the signals of
246 carbon positions G₄ and A₄ were located at 150.3 ppm, and were assigned to C=C groups in
247 both nucleotides bases. This signal was also present in the RNA@Mt hybrids, but shifted to
248 151.5 ppm. The signal at 165.4 ppm associated with the carbon at position 4 in cytosine (-
249 (NH₂) C=N) group, shifted to 166.4, 166.6, 166.4, and 166.5 ppm, in the RNA@Na-Mt,
250 RNA@Ca-Mt, RNA@Mg-Mt, and RNA@Sr-Mt, respectively. The other well-individualized
251 signals did not shift as much.



252

253 **Figure 5.** ^{13}C NMR spectra of the RNA and RNA@Mt hybrids obtained at pH 2.9-3.1 (The
 254 symbol C' represents the carbons present in the ribose group and U₅, for example, represents
 255 the carbon 5 in the uracil nitrogen base).

256 **Table 1.** ^{13}C chemical shifts of RNA and RNA@clay hybrids in pH 2.9-3.1*.

RNA	RNA@Na- Mt	RNA@Ca- Mt	RNA@Mg- Mt	RNA@Sr- Mt	Attributions
67.2	67.0	67.1	67.1	67.1	C5 ^a
74.7	74.7	74.8	74.8	74.9	C3 ^b
85.0	85.0	85.0	85.0	85.0	C4 ^a
91.2	91.4	91.2	91.4	91.5	C1 ^b
102.5	102.7	102.6	102.6	102.4	U5 ^b
119.0	119.0	119.0	119.0	119.0	A5 and G5 ^b
144.1	143.9	144.0	143.9	143.8	C6 and U6 ^{b,d}
150.3	151.5	151.5	151.5	151.5	G4 and A4 ^b
155.4	-	-	-	-	A2 and A6 ^{b,c}
159.8	159.7	159.5	159.5	160.0	G6 ^d
165.4	166.4	166.6	166.4	166.5	C4 ^b

257 *Chemical Shifts in ppm. ^a(Rodrigues et al., 2019); ^b(Chang et al., 1982); ^c(Fujiwara et al., 1995);
 258 ^d(Lapper et al., 1973). C' refers the carbons of the ribose group; A4, C4, U4 and G4 for example, refer
 259 to carbon 4 in the adenine, cytosine, uracil, and guanine nitrogen base, respectively.

260

261 3.4. Thermogravimetry

262

263 TG and DTG curves of the solids before and after RNA adsorption at pH 2.9-3.1 are
 264 presented in Figure SM-3, and summarized in Table SM1. It was hoped that the amount of
 265 intercalated RNA could be estimated by integrating the weight losses after 200°C and
 266 correcting for the weight loss of the raw montmorillonite clay. Some thermal events
 267 attributable to the degradation of RNA are indeed apparent between 200 and 460°C, but
 268 organic matter elimination is not complete even at 1000°C, so that the amounts tabulated are
 269 to be interpreted as lower bounds. They appear to be only little sensitive to the nature of the
 270 compensation cation, or even to its charge.

271

272 **4. Discussion**

273 *XRD diffraction*

274 The XRD patterns of the sodium montmorillonite confirm the expected dioctahedral
275 character of the sample according to the $2\theta = 62.13^\circ$ reflection, indexed (060) plane; in other
276 words, they indicate the predominance of trivalent cations in the octahedral sheet of Na-Mt
277 (Moore and Reynolds, 1997; Reinholdt et al., 2001, 2005). For the exchanged samples, the
278 observation of the (001) reflections at 1.56 nm for all samples are compatible with a two-layer
279 hydrate in the interlayer, as compared to a one-layer hydrate in the starting material (Cases et
280 al., 1997; Cavalcante et al., 2016; Chang et al., 2018).

281 After RNA adsorption, there is no intercalation of bulky species in the interlayer space
282 in the pH 6.2-6.5 systems, as the d_{001} still corresponds to a two-water layer hydrate. The
283 possibility of intercalation strongly depends on the electrostatic interactions between the clay
284 mineral layers (negatively charged) and the molecule to be intercalated. Individual
285 nucleotides exhibit two or three acid-basic couples due to the protonation/deprotonation of
286 nucleobase nitrogens and of the bridging phosphate P-OH (Martin, 1985; Feuillie et al.,
287 2013). Deprotonation of the heterocycle NH group is possible for GMP and UMP nucleotides
288 ($pK_a = 9.4$ to 9.5) but this equilibrium is not active in our pH conditions. The nucleobases
289 may be protonated in the cases of AMP (N1, $pK_a = 3.84$), CMP (N3, $pK_a = 4.33$) and GMP
290 (N7, $pK_a = 2.48$) (Feuillie et al., 2015). This part of the nucleotides would then be mostly
291 neutral at pH 6.2 to 6.5, while at pH 2.9 to 3.1, the majority of AMP and CMP groups, and a
292 minority of the GMP (20 to 30%) would be protonated. Finally, the phosphate group has a
293 pK_a of the order of 0.5 and is always deprotonated in our conditions.

294 Thus, in a neutral medium, each nucleotide residue would bear a net negative charge
295 of -1 and the intercalation of the biopolymer would be electrostatically disfavored because of

296 repulsive interactions with the negative clay mineral layers, since in all pH conditions,
297 montmorillonite has a negative charge (Saka and Güler, 2006; Yukselen and Erzin, 2008; Liu
298 et al., 2017; Şans et al., 2017; Guillermin et al., 2019). It is therefore likely that RNA
299 molecules at pH 6.2-6.5 are adsorbed on the external surface and edges of the clay mineral
300 samples (Mignon et al., 2009; Mignon and Sodupe, 2012). In addition, the cations (Na^+ , Ca^{2+} ,
301 Mg^{2+} and Sr^{2+}) may be contributing to adsorption, by creating “ion bridges” between the
302 negative surface of montmorillonite and the phosphate groups present in RNA. A similar
303 mechanism was invoked for the adsorption of DNA in montmorillonite in the presence of
304 different cations (Sheng et al., 2019).

305 For the system at pH 2.9-3.1, higher basal reflections were observed for all samples,
306 indicating the intercalation of a rather large biomolecule in the interlayer space of the clay
307 mineral. The occurrence of intercalation is associated with the partial protonation of the
308 nitrogen bases in the RNA nucleotides at pH values lower than their pKa. With the pKa
309 values listed above, and supposing that the four possible nucleotide monomers have similar
310 abundances in the RNA chain, it is easy to calculate that at pH 2.9-3.1, the chain bears a
311 charge that is reduced by over one half with respect to pH 6.2-6.5 – about 0.48 negative
312 charges per monomer. In these conditions, electrostatic repulsion between the RNA chain and
313 the negatively charged surface is reduced, permitting intercalation. These interpretations are
314 compatible with other studies in RNA adsorption (Greaves and Wilson, 1969; Jelavić et al.,
315 2017) and also studies about the adsorption of the nitrogen bases (Carneiro et al., 2011) and
316 nucleotides (Pedreira-Segade et al., 2016) on montmorillonite. Similar results were observed
317 in the RNA intercalation in montmorillonite in an acidic medium (pH 5 to 3.5) (Greaves and
318 Wilson, 1969). Other studies observed no displacement of the basal plane in torula yeast
319 RNA/Mg-smectite (Viennet et al., 2020) and DNA/ion-exchanged Mt (Li^+ , Na^+ , Mg^{2+} , Ca^{2+} ,
320 Fe^{3+} and Al^{3+}) Mt (Xie et al., 2019), but they were not conducted at low pH.

321 It is obvious that what is intercalated is not the intact torula yeast RNA, which has an
322 intricate ternary structure and exists in solution as a Y-shaped molecule (Tripathi et al., 2017)
323 with a 30 nm gyration radius (Manzano and Zydney, 2017). Indeed, a double strand of nucleic
324 acid has a diameter of about 26 Å, and consequently, even a single strand lying in the
325 interlayer with its nucleobases perpendicular to the clay layers would give an interlayer
326 spacing of about 13 Å, significantly higher than the values we observe. This is why in the
327 structural sketch of intercalated RNA we propose in Figure 6, the RNA strand is represented
328 with the bases lying flat in the interlayer. This would involve a strong degree of RNA
329 deformation; therefore, it is likely that the whole RNA molecule does not enter the interlayer.
330 It is proposed that only fragments of the RNA chain are intercalated, while the rest of the
331 molecule may be adsorbed on the surface or edges of the Mt. A similar adsorption
332 mechanism has been documented for other biomacromolecules in Mt, such as enzymes
333 (Sanjay and Sugunan, 2006; Gopinath and Sugunan, 2007).

334 *Infrared spectroscopy*

335 At both pHs, new bands were observed in the FTIR spectra of samples after the
336 absorption of RNA. For example, at pH 6.2-6.5, bands assigned to ring vibrations and in-
337 plane C-O-H deformation of ribose were observed. At pH 2.9-3.1, new bands assigned to
338 C=O and PO₂⁻ stretching were apparent. Furthermore, changes in the position of the PO₂⁻
339 band were observed. This shift is probably associated with distortions in the RNA molecule,
340 possibly caused by the interactions of cations with phosphate groups (Duguid et al., 1993;
341 Andrushchenko and Bouř, 2009; Pedreira-Segade et al., 2018). It is likely that the clay/RNA
342 interaction simultaneously includes several contributions from different local interactions
343 such as H-bonds. It may be relevant from this point of view that the stretching vibration of the
344 clay layer structural O-H shifts by a few cm⁻¹, which may be indicative of their implication in

345 H-bonding (Schnetzer et al., 2017), but a more precise study would be needed to identify H-
346 bonds with confidence.

347 *²⁷Al, ¹³C and ³¹P solid state NMR*

348

349 ²⁷Al NMR spectra in all precursor samples presented characteristic chemical shifts at
350 3.9 and 69.1 ppm related to hexacoordinated (Al 6-c) and tetraordinated (Al 4-c) aluminum
351 located in octahedral and tetrahedral sheets of the Mt, respectively (Cadars et al., 2012; Marsh
352 et al., 2018). Another chemical shift corresponding to the Al 4-c environment was observed in
353 both spectra at 55 ppm and can be attributed to small impurities of amorphous
354 aluminosilicate, also observed in the literature for synthetic (Cadars et al., 2012) and natural
355 (Garg and Skibsted, 2014) montmorillonites. In the RNA@cations-Mt samples (Figure 3ii),
356 no change was observed with respect to cations-Mt, indicating the absence of interaction
357 between the biomolecule and Al sites in the Mt.

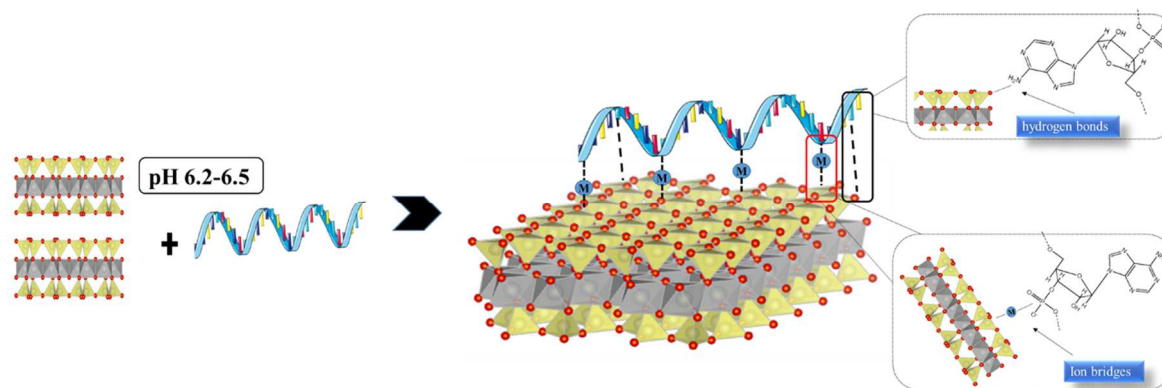
358 As regards the ³¹P spectrum of RNA, Figure 4i, there are surprisingly few literature
359 results available for comparison. Solution studies of short RNA sequences (Legault and Pardi,
360 1994; Maderia et al., 2000) revealed a series of narrow peaks in the (+2.0, -2.0) ppm range
361 corresponding to all different phosphodiester bridges in the RNA chain. In the solid state, the
362 loss of resolution may produce a signal such as the one we are observing. For the
363 RNA@cations-Mt samples, a strong new component appeared. This finding is quite
364 unexpected since the shift is comparable to the chemical shift difference separating the Q⁰
365 signal in monophosphate from the Q¹ in diphosphate. The formation of diphosphate seems
366 unlikely however, as it would require a breakdown and rearrangement of the RNA structure.
367 Another possibility is that the new signal could correspond to the effect of the adsorption
368 interaction on the bridging phosphate groups. Among likely interactions, only coordinative
369 bonds to metal cations would be expected to result in such shifts. Intuitively, however, they

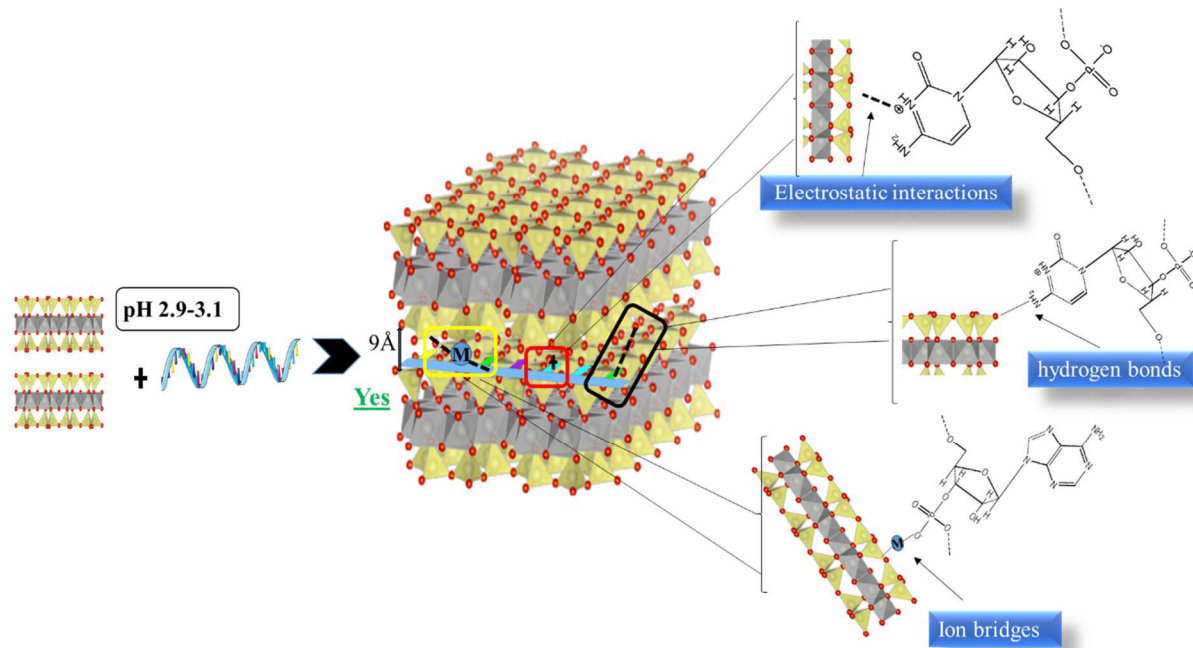
370 would also be expected to induce a decrease in electron density in the phosphate moiety, and
371 therefore a downfield shift (increase in chemical shift values) – the opposite of the effect
372 observed here. The already quoted study by Maderia et al (2000) indeed reports shifts of
373 several ppm when modified hairpin RNA is contacted with Cd^{2+} or Mg^{2+} cations. For
374 different RNA structures, they can be either upfield or downfield. The authors could not
375 provide any clear explanation for the upfield shifts; they supposed that the affected phosphate
376 groups did not directly coordinate to the cations, but were indirectly affected through changes
377 in RNA conformations. We will not speculate any further on the reasons for the new signal
378 observed here, except to say that it reveals a strong RNA/clay mineral interaction. One can
379 also note that in at least three of the four samples, there are indications of a third, even more
380 upfield shifted component in the ^{31}P spectrum; attempts at signal deconvolution necessitated
381 the introduction of a component at -14 to -17 ppm. The hypothesis of strong deformations of
382 the RNA chain is in line with the structural picture deduced from XRD.

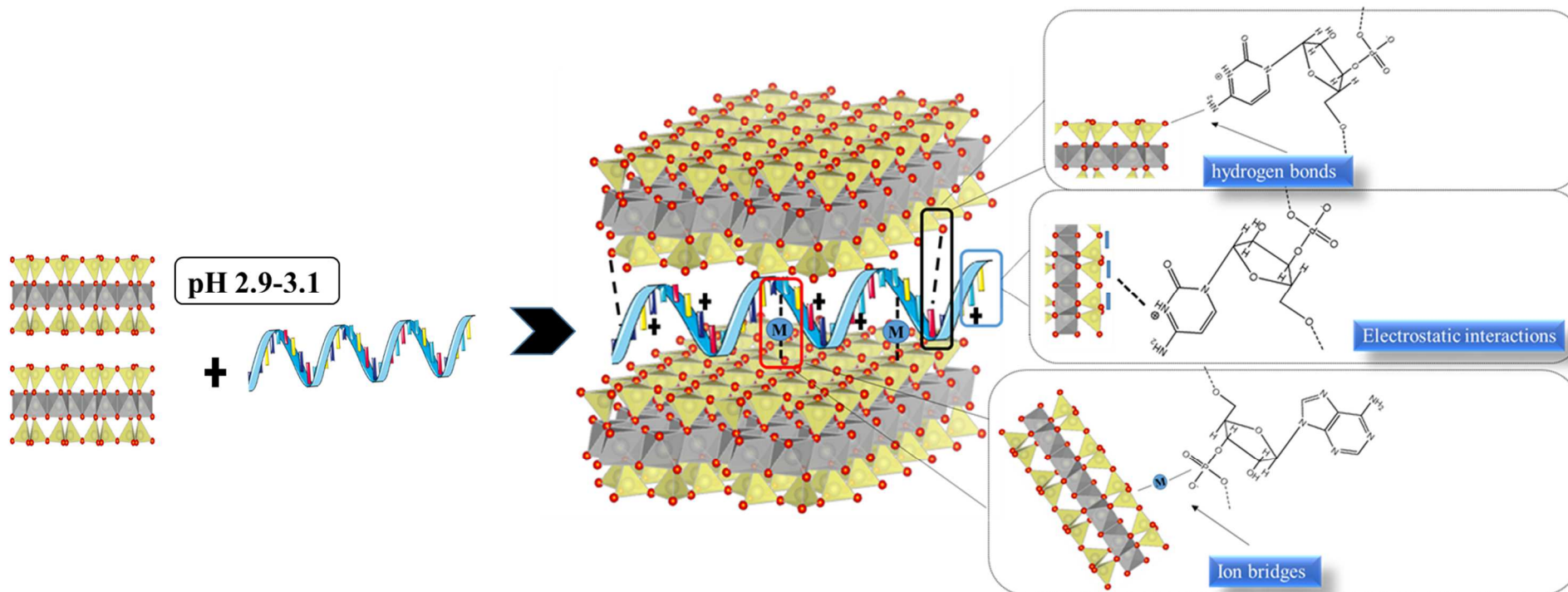
383 The ^{13}C NMR spectra show chemical shifts values that are practically the same for
384 the different montmorillonites. This suggests that the nucleotide bases, mainly adenine and
385 cytosine, can be protonated in an acidic medium (pH 2.9-3.1). These results are in keeping
386 with calculations based on the pKa values. They corroborate the FTIR and XRD results,
387 indicating that the protonation of these moieties induces hydrogen bonds and electrostatic
388 interactions with the montmorillonite surface.

389 Figure 6 sketches a model of the RNA-clay composites that is compatible with the
390 information from XRD, IR and ^{13}C and ^{31}P NMR.

391







394

395

Figure 6. Illustrative scheme for proposed interactions between fragment of RNA and montmorillonite in neutral and acidic medium.

396 **5. Conclusions**

397

398 We have investigated the interaction of an RNA-derived molecule with synthetic
399 montmorillonites having different cations in their interlayer space. The systems were prepared
400 in both neutral and acidic media.

401 The interaction of the biomolecule with montmorillonites was pH-dependent: the
402 intercalation of RNA in the interlayer space of montmorillonite was largely controlled by
403 electrostatic interactions. At close to neutral pH, the RNA molecules have a significant
404 negative charge and are prevented from entering the interlayer space by electrostatic repulsion
405 from the clay mineral layers. It is likely that RNA is adsorbed on edge sites, maybe with
406 compensating cations acting as ions bridges.

407 At lower pH values, extensive intercalation occurs, as evidenced by the value of basal
408 spacing observed in XRD. Indeed, the nucleobases are then expected to be partly protonated,
409 resulting in significantly lower negative charges on the RNA molecules. The driving force for
410 intercalation could include contributions of localized electrostatic interactions (between the
411 positively charged aromatic nuclei and the negatively charged clay mineral layers), probably
412 accompanied by H-bonding, and also of coordinative bonding with the interlayer cations.
413 Some authors have suggested that at pH close to 7, van der Waals interactions between the
414 montmorillonite layers and the purine and pyrimidine bases of the nucleotides may also be
415 acting (Kawamura and Ferris, 1999; Ferris, 2006).

416 Indeed, both FTIR and ¹³C NMR indicate small but significant modifications of the
417 ring carbon atoms local environment. FTIR also shows a rather important shift of the
418 phosphate band. Taken together, these results suggest that both groups are involved in the
419 interaction mechanism. ³¹P NMR shows a surprisingly strong effect of adsorption on the

420 phosphates, but the direction of the shift does not seem compatible with a coordination to the
421 electropositive compensating cations. Rather, it might be indicative of important
422 configuration changes induced by the intercalation of the RNA backbone into a constrained
423 space.

424 These results indicate that RNA oligomers and polymers may have interacted
425 effectively with clay minerals, such as montmorillonite, in an acidic medium on the primitive
426 Earth. Such an RNA/montmorillonite interaction may have stabilized and protected RNA
427 molecules from an environment of likely hostile conditions on the primitive earth, such as
428 high UV radiation.

429 **Acknowledgements**

430 The authors thank CAPES and CNPq (grants 310921-2017-1 and 431727/2016-3) for
431 the financial support.

432

433 **References**

434 Akouche, M., Jaber, M., Zins, E.L., Maurel, M.C., Lambert, J.F., Georgelin, T., 2016.
435 Thermal Behavior of d-Ribose Adsorbed on Silica: Effect of Inorganic Salt
436 Coadsorption and Significance for Prebiotic Chemistry. *Chem. - A Eur. J.* 22,
437 15834–15846. <https://doi.org/10.1002/chem.201601418>

438 Andrushchenko, V., Bouř, P., 2009. Infrared absorption detection of metal ion-
439 deoxyguanosine monophosphate binding: Experimental and theoretical study. *J.*
440 *Phys. Chem. B* 113, 283–291. <https://doi.org/10.1021/jp8058678>

441 Banyay, M., Sarkar, M., Gräslund, A., 2003. A library of IR bands of nucleic acids in
442 solution. *Biophys. Chem.* 104, 477–488. [https://doi.org/10.1016/S0301-](https://doi.org/10.1016/S0301-4622(03)00035-8)
443 [4622\(03\)00035-8](https://doi.org/10.1016/S0301-4622(03)00035-8)

444 Benedetti, Edoardo, Bramanti, E., Papineschi, F., Rossi, I., Benedetti, Enzo, 1997.

445 Determination of the relative amount of nucleic acids and proteins in leukemic and
446 normal lymphocytes by means of fourier transform infrared microspectroscopy.
447 *Appl. Spectrosc.* 51, 792–797. <https://doi.org/10.1366/0003702971941304>

448 Benetoli, L.O.D.B., De Santana, H., Zaia, C.T.B. V, Zaia, D.A.M., 2008. Adsorption of
449 nucleic acid bases on clays: An investigation using Langmuir and Freundlich
450 isotherms and FT-IR spectroscopy. *Monatshefte fur Chemie* 139, 753–761.
451 <https://doi.org/10.1007/s00706-008-0862-z>

452 Bizovská, V., Jankovič, Ľ., Madejová, J., 2018. Montmorillonite modified with
453 unconventional surfactants from the series of octylammonium-based cations:
454 Structural characterization and hydration properties. *Appl. Clay Sci.* 158, 102–112.
455 <https://doi.org/10.1016/j.clay.2018.03.013>

456 Black, C.B., Huang, H.W., Cowan, J.A., 1994. Biological coordination chemistry of
457 magnesium, sodium, and potassium ions. Protein and nucleotide binding sites.
458 *Coord. Chem. Rev.* 135–136, 165–202. [https://doi.org/10.1016/0010-](https://doi.org/10.1016/0010-8545(94)80068-5)
459 [8545\(94\)80068-5](https://doi.org/10.1016/0010-8545(94)80068-5)

460 Cadars, S., Guégan, R., Garaga, M.N., Bourrat, X., Le Forestier, L., Fayon, F., Huynh,
461 T.V., Allier, T., Nour, Z., Massiot, D., 2012. New insights into the molecular
462 structures, compositions, and cation distributions in synthetic and natural
463 montmorillonite clays. *Chem. Mater.* 24, 4376–4389.
464 <https://doi.org/10.1021/cm302549k>

465 Carneiro, C.E.A., Berndt, G., de Souza Junior, I.G., de Souza, C.M.D., Paesano, A., da
466 Costa, A.C.S., di Mauro, E., de Santana, H., Zaia, C.T.B. V., Zaia, D.A.M., 2011.
467 Adsorption of Adenine, Cytosine, Thymine, and Uracil on Sulfide-Modified
468 Montmorillonite: FT-IR, Mössbauer and EPR Spectroscopy and X-Ray
469 Diffractometry Studies. *Orig. Life Evol. Biosph.* 41, 453–468.
470 <https://doi.org/10.1007/s11084-011-9244-3>

471 Carrascoza Mayén, J. F.; Rydzewski, J.; Szostak, N.; Blazewicz, J.; Nowak, W.,
472 Prebiotic Soup Components Trapped in Montmorillonite Nanoclay Form New
473 Molecules: Car-Parrinello Ab Initio Simulations. *Life* 2019, 9,
474 doi: 10.3390/life9020046.

475 Cases, J.M., Berend, I., Francois, M., Uriot, J.P., Michot, L.J., Thomas, F., 1997.
476 Mechanism of adsorption and desorption of water vapor by homoionic
477 montmorillonite. 3. The Mg^{2+} , Ca^{2+} , Sr^{2+} and Ba^{2+} exchanged forms. *Clays Clay*
478 *Miner.* 45, 8–22.

479 Cavalcante, M.S., Paz, S.P.A., Angélica, R.S., Ito, E.N., Freitas Neves, R., 2016.
480 Organophilization of a Brazilian Mg-montmorillonite without prior sodium
481 activation. *Clay Miner.* 51, 39–54. <https://doi.org/10.1180/claymin.2016.051.1.04>

482 Cavalcanti, G.R.S., Rodrigues, F., Zhuang, G., Balme, S., Janot, J.M., Fonseca, M.G.,
483 Jaber, M., 2021. Inorganic-organic hybrid pigments based on carminic acid and
484 clay minerals. *Dye. Pigment.* 190. <https://doi.org/10.1016/j.dyepig.2021.109306>

485 Chang, C. jer, Diaz, L.E., Woolfenden, W.R., Grant, D.M., 1982. Solid-State Carbon-13
486 Nuclear Magnetic Resonance Study of Ribonucleosides and Ribonucleic Acid. *J.*
487 *Org. Chem.* 47, 5318–5321. <https://doi.org/10.1021/jo00148a018>

488 Chang, P.H., Jiang, W.T., Li, Z., 2018. Mechanism of tyramine adsorption on Ca-
489 montmorillonite. *Sci. Total Environ.* 642, 198–207.
490 <https://doi.org/10.1016/j.scitotenv.2018.05.190>

491 Costa, T.M.H., Gallas, M.R., Benvenuti, E. V., Da Jornada, J.A.H., 1997. Infrared and
492 thermogravimetric study of high pressure consolidation in alkoxide silica gel
493 powders. *J. Non. Cryst. Solids* 220, 195–201. [https://doi.org/10.1016/S0022-](https://doi.org/10.1016/S0022-3093(97)00236-6)
494 [3093\(97\)00236-6](https://doi.org/10.1016/S0022-3093(97)00236-6)

495 da Silva, J.C.S., França, D.B., Rodrigues, F., Oliveira, D.M., Trigueiro, P., Silva Filho,
496 E.C., Fonseca, M.G., 2021. What happens when chitosan meets bentonite under
497 microwave-assisted conditions? Clay-based hybrid nanocomposites for dye
498 adsorption. *Colloids Surfaces A Physicochem. Eng. Asp.* 609, 125584.
499 <https://doi.org/10.1016/j.colsurfa.2020.125584>

500 Duguid, J., Bloomfield, V.A., Benevides, J., Thomas, G.J., 1993. Raman spectroscopy
501 of DNA-metal complexes. I. Interactions and conformational effects of the divalent
502 cations: Mg, Ca, Sr, Ba, Mn, Co, Ni, Cu, Pd, and Cd. *Biophys. J.* 65, 1916–1928.
503 [https://doi.org/10.1016/S0006-3495\(93\)81263-3](https://doi.org/10.1016/S0006-3495(93)81263-3)

- 504 Eder, A.H., Rode, B.M., 1994. Influence of alkali- and alkaline-earth-metal cations on
505 the “salt-induced peptide formation” reaction. *J. Chem. Soc. Dalt. Trans.* 1125–
506 1130. <https://doi.org/10.1039/DT9940001125>
- 507 Escamilla-Roa, E., Huertas, F.J., Hernández-Laguna, A., Sainz-Díaz, C.I., 2017. A DFT
508 study of the adsorption of glycine in the interlayer space of montmorillonite. *Phys.*
509 *Chem. Chem. Phys.* 19, 14961–14971. <https://doi.org/10.1039/c7cp02300f>
- 510 Ferris, J.P., 2006. Montmorillonite-catalysed formation of RNA oligomers: The
511 possible role of catalysis in the origins of life. *Philos. Trans. R. Soc. B Biol. Sci.*
512 361, 1777–1786. <https://doi.org/10.1098/rstb.2006.1903>
- 513 Feuillie, C., Daniel, I., Michot, L.J., Pedreira-Segade, U., 2013. Adsorption of
514 nucleotides onto Fe-Mg-Al rich swelling clays. *Geochim. Cosmochim. Acta* 120,
515 97–108. <https://doi.org/10.1016/j.gca.2013.06.021>
- 516 Feuillie, C., Sverjensky, D.A., Hazen, R.M., 2015. Attachment of ribonucleotides on α -
517 alumina as a function of pH, ionic strength, and surface loading. *Langmuir* 31, 240–
518 248. <https://doi.org/10.1021/la504034k>
- 519 Fornaro, T., Brucato, J.R., Feuillie, C., Sverjensky, D.A., Hazen, R.M., Brunetto, R.,
520 D’Amore, M., Barone, V., 2018. Binding of Nucleic Acid Components to the
521 Serpentine-Hosted Hydrothermal Mineral Brucite. *Astrobiology* 18, 989–1007.
522 <https://doi.org/10.1089/ast.2017.1784>
- 523 França, D.B., Trigueiro, P., Silva Filho, E.C., Fonseca, M.G., Jaber, M., 2020.
524 Monitoring diclofenac adsorption by organophilic alkylpyridinium bentonites.
525 *Chemosphere* 242, 125109. <https://doi.org/10.1016/j.chemosphere.2019.125109>
- 526 Franchi, M., Ferris, J.P., Gallori, E., 2003. Cations as mediators of the adsorption of
527 nucleic acids on clay surfaces in prebiotic environments. *Orig. Life Evol. Biosph.*
528 33, 1–16. <https://doi.org/10.1023/A:1023982008714>
- 529 Fujiwara, T., Sugase, K., Akutsu, H., Kainosho, M., Ono, A., Ono, A.M., 1995. ^{13}C —
530 ^{13}C and ^{13}C — ^{15}N Dipolar Correlation NMR of Uniformly Labeled Organic
531 Solids for the Complete Assignment of Their ^{13}C and ^{15}N Signals: An
532 Application to Adenosine. *J. Am. Chem. Soc.* 117, 11351–11352.

533 <https://doi.org/10.1021/ja00150a038>

534 Garg, N., Skibsted, J., 2014. Thermal activation of a pure montmorillonite clay and its
535 reactivity in cementitious systems. *J. Phys. Chem. C* 118, 11464–11477.
536 <https://doi.org/10.1021/jp502529d>

537 Gopinath, S., Sugunan, S., 2007. Enzymes immobilized on montmorillonite K 10:
538 Effect of adsorption and grafting on the surface properties and the enzyme activity.
539 *Appl. Clay Sci.* 35, 67–75. <https://doi.org/10.1016/j.clay.2006.04.007>

540 Greaves, M.P., Wilson, M.J., 1969. The adsorption of nucleic acids by montmorillonite.
541 *Soil Biol. Biochem.* 1, 317–323. [https://doi.org/10.1016/0038-0717\(69\)90014-5](https://doi.org/10.1016/0038-0717(69)90014-5)

542 Guillermin, D., Debrouse, T., Trigueiro, P., de Viguerie, L., Rigaud, B., Morlet-Savary,
543 F., Balme, S., Janot, J.M., Tielens, F., Michot, L., Lalevee, J., Walter, P., Jaber,
544 M., 2019. New pigments based on carminic acid and smectites: A molecular
545 investigation. *Dye. Pigment.* 160, 971–982.
546 <https://doi.org/10.1016/j.dyepig.2018.07.021>

547 Gujjari, A., Rodriguez, B. V., Pescador, J., Maeder, C., Beall, G.W., Lewis, L.K., 2018.
548 Factors affecting the association of single- and double-stranded RNAs with
549 montmorillonite nanoclays. *Int. J. Biol. Macromol.* 109, 551–559.
550 <https://doi.org/10.1016/j.ijbiomac.2017.12.124>

551 Hao, J., Mokhtari, M., Pedreira-Segade, U., Michot, L.J., Daniel, I., 2019. Transition
552 Metals Enhance the Adsorption of Nucleotides onto Clays: Implications for the
553 Origin of Life. *ACS Earth Sp. Chem.* 3, 109–119.
554 <https://doi.org/10.1021/acsearthspacechem.8b00145>

555 Hashizume, H., van der Gaast, S., Theng, B.K.G., 2010. Adsorption of adenine,
556 cytosine, uracil, ribose, and phosphate by Mg-exchanged montmorillonite. *Clay*
557 *Miner.* 45, 469–475. <https://doi.org/10.1180/claymin.2010.045.4.469>

558 Izawa, M.R.M., Nesbitt, H.W., MacRae, N.D., Hoffman, E.L., 2010. Composition and
559 evolution of the early oceans: Evidence from the Tagish Lake meteorite. *Earth*
560 *Planet. Sci. Lett.* 298, 443–449. <https://doi.org/10.1016/j.epsl.2010.08.026>

- 561 Jaber, M., Georgelin, T., Bazzi, H., Costa-Torro, F., Lambert, J.-F., Bolbach, G.,
562 Clodic, G., 2014. Selectivities in Adsorption and Peptidic Condensation in the
563 (Arginine and Glutamic Acid)/Montmorillonite Clay System. *J. Phys. Chem. C*
564 118, 25447–25455. <https://doi.org/10.1021/jp507335e>
- 565 Jaber, M., Miehé-Brendlé, J., 2008. Synthesis, characterization and applications of 2:1
566 phyllosilicates and organophyllosilicates: Contribution of fluoride to study the
567 octahedral sheet. *Microporous Mesoporous Mater.* 107, 121–127.
568 <https://doi.org/10.1016/j.micromeso.2007.02.047>
- 569 Jaber, M., Miehé-Brendlé, J., 2005. Influence du milieu de synthèse sur la cristallisation
570 de saponite: Proposition de mécanisme réactionnel en milieux acide et basique.
571 *Comptes Rendus Chim.* 8, 229–234. <https://doi.org/10.1016/j.crci.2004.10.025>
- 572 James Cleaves, H., Michalkova Scott, A., Hill, F.C., Leszczynski, J., Sahai, N., Hazen,
573 R., 2012. Mineral-organic interfacial processes: Potential roles in the origins of
574 life. *Chem. Soc. Rev.* 41, 5502–5525. <https://doi.org/10.1039/c2cs35112a>
- 575 Jelavić, S., Tobler, D.J., Hassenkam, T., De Yoreo, J.J., Stipp, S.L.S., Sand, K.K., 2017.
576 Prebiotic RNA polymerisation: energetics of nucleotide adsorption and
577 polymerisation on clay mineral surfaces. *Chem. Commun.* 53, 12700–12703.
578 <https://doi.org/10.1039/C7CC04276K>
- 579 Kawamura, K., Ferris, J.P., 1999. Clay catalysis of oligonucleotide formation: Kinetics
580 of the reaction of the 5'-phosphorimidazolides of nucleotides with the non-basic
581 heterocycles uracil and hypoxanthine. *Orig. Life Evol. Biosph.* 29, 563–591.
582 <https://doi.org/10.1023/A:1006648524187>
- 583 Kim, S.H., Sussman, J.L., Suddath, F.L., Quigley, G.J., McPherson, A., Wang, A.H.,
584 Seeman, N.C., RICH, A., 1974. The general structure of transfer RNA molecules.
585 *Proc. Natl. Acad. Sci. U. S. A.* 71, 4970–4974.
586 <https://doi.org/10.1073/pnas.71.12.4970>
- 587 Kumar, A., Singh, B., 2013. Zn²⁺-induced folding of RNA to produce honeycomb-like
588 RNA-mediated fluorescing Zn²⁺/PbSe nanostructures. *J. Phys. Chem. C* 117,
589 5386–5396. <https://doi.org/10.1021/jp309822w>

590 Lapper, R.D., Mantsch, H.H., Smith, I.C.P., 1973. A Carbon-13 Nuclear Magnetic
591 Resonance Study of the Conformations of 3',5'-Cyclic Nucleotides. *J. Am. Chem.*
592 *Soc.* 95, 2878–2880. <https://doi.org/10.1021/ja00790a024>

593 Lawless, J. G.; Banin, A.; Church, F. M.; Mazzurco, J.; Huff, R.; Kao, J.; Cook, A.;
594 Lowe, T.; Orenberg, J. B.; Eelson, E., pH Profile of the Adsorption of Nucleotides
595 onto Montmorillonite.1. Selected Homoionic Clays. *Orig. Life Evol. Biosph.* **1985**,
596 *15* (2), 77-88.

597

598 Legault, P., Pardi, A., 1994. ³¹P Chemical Shift as a Probe of Structural Motifs in
599 RNA. *J. Magn. Reson. Ser. B.* <https://doi.org/10.1006/jmrb.1994.1012>

600 Leonarski, F., D'Ascenzo, L., Auffinger, P., 2017. Mg²⁺ ions: Do they bind to
601 nucleobase nitrogens? *Nucleic Acids Res.* 45, 987–1004.
602 <https://doi.org/10.1093/nar/gkw1175>

603 Lepoitevin, M., Jaber, M., Guégan, R., Janot, J.M., Dejardin, P., Henn, F., Balme, S.,
604 2014. BSA and lysozyme adsorption on homoionic montmorillonite: Influence of
605 the interlayer cation. *Appl. Clay Sci.* 95, 396–402.
606 <https://doi.org/10.1016/j.clay.2014.05.003>

607 Liu, J., Zhao, Y., Li, H., Chen, T., Song, S., 2017. Stability of Na-montmorillonite
608 suspension in the presence of different cations and valences. *J. Dispers. Sci.*
609 *Technol.* 38, 1035–1040. <https://doi.org/10.1080/01932691.2016.1218344>

610 Madejová, J., Gates, W.P., Petit, S., 2017. IR Spectra of Clay Minerals, Developments
611 in Clay Science. Elsevier. <https://doi.org/10.1016/B978-0-08-100355-8.00005-9>

612 Maderia, M., Horton, T.E., DeRose, V.J., 2000. Metal Interactions with a GAAA RNA
613 Tetraloop Characterized by ³¹P NMR and Phosphorothioate Substitutions †.
614 *Biochemistry* 39, 8193–8200. <https://doi.org/10.1021/bi000140l>

615 Manzano, I., Zydney, A.L., 2017. Quantitative study of RNA transmission through
616 ultrafiltration membranes. *J. Memb. Sci.* 544, 272–277.
617 <https://doi.org/10.1016/j.memsci.2017.09.042>

- 618 Marsh, A., Heath, A., Patureau, P., Evernden, M., Walker, P., 2018. Alkali activation
619 behaviour of un-calcined montmorillonite and illite clay minerals. *Appl. Clay Sci.*
620 166, 250–261. <https://doi.org/10.1016/j.clay.2018.09.011>
- 621 Martin, R.B., 1985. Nucleoside Sites for Transition Metal Ion Binding. *Acc. Chem. Res.*
622 18, 32–38. <https://doi.org/10.1021/ar00110a001>
- 623 Mignon, P., Sodupe, M., 2012. Theoretical study of the adsorption of DNA bases on the
624 acidic external surface of montmorillonite. *Phys. Chem. Chem. Phys.* 14, 945–954.
625 <https://doi.org/10.1039/c1cp22454a>
- 626 Mignon, P., Ugliengo, P., Sodupe, M., 2009. Theoretical study of the adsorption of
627 RNA/DNA bases on the external surfaces of Na⁺-montmorillonite. *J. Phys. Chem.*
628 C 113, 13741–13749. <https://doi.org/10.1021/jp901699q>
- 629 Moore, D.M., Reynolds, R.C., 1997. X-Ray Diffraction and the Identification and
630 Analysis of Clay Minerals. Oxford University Press, New York.
- 631 Pedreira-Segade, U., Feuillie, C., Pelletier, M., Michot, L.J., Daniel, I., 2016.
632 Adsorption of nucleotides onto ferromagnesian phyllosilicates: Significance for the
633 origin of life. *Geochim. Cosmochim. Acta* 176, 81–95.
634 <https://doi.org/10.1016/j.gca.2015.12.025>
- 635 Pedreira-Segade, U., Michot, L.J., Daniel, I., 2018. Effects of salinity on the adsorption
636 of nucleotides onto phyllosilicates. *Phys. Chem. Chem. Phys.* 20, 1938–1952.
637 <https://doi.org/10.1039/c7cp07004g>
- 638 Pentrák, M., Bizovská, V., Madejová, J., 2012. Near-IR study of water adsorption on
639 acid-treated montmorillonite. *Vib. Spectrosc.* 63, 360–366.
640 <https://doi.org/10.1016/j.vibspec.2012.07.012>
- 641 Pentrák, M., Hronský, V., Pálková, H., Uhlík, P., Komadel, P., Madejová, J., 2018.
642 Alteration of fine fraction of bentonite from Kopernica (Slovakia) under acid
643 treatment: A combined XRD, FTIR, MAS NMR and AES study. *Appl. Clay Sci.*
644 163, 204–213. <https://doi.org/10.1016/j.clay.2018.07.028>
- 645 Pyle, A.M., 2002. Metal ions in the structure and function of RNA. *J. Biol. Inorg.*

646 Chem. 7, 679–690. <https://doi.org/10.1007/s00775-002-0387-6>

647 Reinholdt, M., Miehé-Brendlé, J., Delmotte, L., Le Dred, R., Tuilier, M.-H., 2005.
648 Synthesis and characterization of montmorillonite-type phyllosilicates in a fluoride
649 medium. *Clay Miner.* 40, 177–190. <https://doi.org/10.1180/0009855054020164>

650 Reinholdt, M., Miehé-Brendlé, J., Delmotte, L., Tuilier, M.-H., le Dred, R., Cortès, R.,
651 Flank, A.-M., 2001. Fluorine Route Synthesis of Montmorillonites Containing Mg
652 or Zn and Characterization by XRD, Thermal Analysis, MAS NMR, and EXAFS
653 Spectroscopy. *Eur. J. Inorg. Chem.* 2001, 2831–2841.
654 [https://doi.org/10.1002/1099-0682\(200111\)2001:11<2831::AID-](https://doi.org/10.1002/1099-0682(200111)2001:11<2831::AID-EJIC2831>3.0.CO;2-6)
655 [EJIC2831>3.0.CO;2-6](https://doi.org/10.1002/1099-0682(200111)2001:11<2831::AID-EJIC2831>3.0.CO;2-6)

656 Rodrigues, F., Georgelin, T., Gabant, G., Rigaud, B., Gaslain, F., Zhuang, G.,
657 Gardênnia da Fonseca, M., Valtchev, V., Touboul, D., Jaber, M., 2019.
658 Confinement and Time Immemorial: Prebiotic Synthesis of Nucleotides on a
659 Porous Mineral Nanoreactor. *J. Phys. Chem. Lett.* 10, 4192–4196.
660 <https://doi.org/10.1021/acs.jpcclett.9b01448>

661 Ruiz-Mirazo, K., Briones, C., De La Escosura, A., 2014. Prebiotic systems chemistry:
662 New perspectives for the origins of life. *Chem. Rev.* 114, 285–366.
663 <https://doi.org/10.1021/cr2004844>

664 Saka, E.E., Güler, C., 2006. The effects of electrolyte concentration, ion species and pH
665 on the zeta potential and electrokinetic charge density of montmorillonite. *Clay*
666 *Miner.* 41, 853–861. <https://doi.org/10.1180/0009855064140224>

667 Sanjay, G., Sugunan, S., 2006. Enhanced pH and thermal stabilities of invertase
668 immobilized on montmorillonite K-10. *Food Chem.* 94, 573–579.
669 <https://doi.org/10.1016/j.foodchem.2004.12.043>

670 Şans, B.E., Güven, O., Esenli, F., Çelik, M.S., 2017. Contribution of cations and layer
671 charges in the smectite structure on zeta potential of Ca-bentonites. *Appl. Clay Sci.*
672 143, 415–421. <https://doi.org/10.1016/j.clay.2017.04.016>

673 Santos, S.S.G., Silva, H.R.M., de Souza, A.G., Alves, A.P.M., da Silva Filho, E.C.,
674 Fonseca, M.G., 2015. Acid-leached mixed vermiculites obtained by treatment with

675 nitric acid. *Appl. Clay Sci.* 104, 286–294.
676 <https://doi.org/10.1016/j.clay.2014.12.008>

677 Schnetzer, F., Johnston, C.T., Premachandra, G.S., Giraud, N., Schuhmann, R.,
678 Thissen, P., Emmerich, K., 2017. Impact of Intrinsic Structural Properties on the
679 Hydration of 2:1 Layer Silicates. *ACS Earth Sp. Chem.* 1, 608–620.
680 <https://doi.org/10.1021/acsearthspacechem.7b00091>

681 Shamsuddin, R.M., Verbeek, C.J.R., Lay, M.C., 2014. Producing protein intercalated
682 bentonite - Equilibrium, kinetics and physical properties of gelatin-bentonite
683 system. *Appl. Clay Sci.* 87, 52–60. <https://doi.org/10.1016/j.clay.2013.11.023>

684 Sheng, X., Qin, C., Yang, B., Hu, X., Liu, C., Waigi, M.G., Li, X., Ling, W., 2019.
685 Metal cation saturation on montmorillonites facilitates the adsorption of DNA via
686 cation bridging. *Chemosphere* 235, 670–678.
687 <https://doi.org/10.1016/j.chemosphere.2019.06.159>

688 Theng, B. K. G., 1982, ‘Clay-polymer interactions: Summary and perspectives’, *Clays*
689 *Clay Miner.* 30, 1–10.

690 Tripathi, M.; Khilari, R.; Thakur, Y.; Verma, B.; Pardhi, M.; Pande, R.,
691 Oxovanadium complex as potential nucleic acid binder. *J. Macromol. Sci. A: Pure*
692 *Appl. Chem.* 2017, 54, 85-90.

693 Trigueiro, P., Pedetti, S., Rigaud, B., Balme, S., Janot, J.-M., dos Santos, I.M.G.,
694 Gougeon, R., Fonseca, M.G., Georgelin, T., Jaber, M., 2018a. Going through the
695 wine fining: Intimate dialogue between organics and clays. *Colloids Surfaces B*
696 *Biointerfaces* 166, 79–88. <https://doi.org/10.1016/j.colsurfb.2018.02.060>

697 Trigueiro, P., Pereira, F.A.R., Guillermin, D., Rigaud, B., Balme, S., Janot, J.-M., dos
698 Santos, I.M.G., Fonseca, M.G., Walter, P., Jaber, M., 2018b. When anthraquinone
699 dyes meet pillared montmorillonite: Stability or fading upon exposure to light?
700 *Dye. Pigment.* 159, 384–394. <https://doi.org/10.1016/j.dyepig.2018.06.046>

701 Tsuboi, M., 1970. Application of Infrared Spectroscopy to Structure Studies of Nucleic
702 Acids. *Appl. Spectrosc. Rev.* 3, 45–90.
703 <https://doi.org/10.1080/05704927008081687>

704 Viennet, J.C., Bernard, S., Le Guillou, C., Jacquemot, P., Delbes, L., Balan, E., Jaber,
705 M., 2020. Influence of the nature of the gas phase on the degradation of RNA
706 during fossilization processes. *Appl. Clay Sci.* 191, 105616.
707 <https://doi.org/10.1016/j.clay.2020.105616>

708 Villafañe-Barajas, S. A.; Baú, J. P. T.; Colín-García, M.; Negrón-Mendoza, A.;
709 Heredia-Barbero, A.; Pi-Puig, T.; Zaia, D. A. M., Salinity Effects on the
710 Adsorption of Nucleic Acid Compounds on Na-Montmorillonite: a Prebiotic
711 Chemistry Experiment. *Orig. Life Evol. Biosph.* 2018, 48 (2), 181-200. DOI:
712 10.1007/s11084-018-9554-9.

713

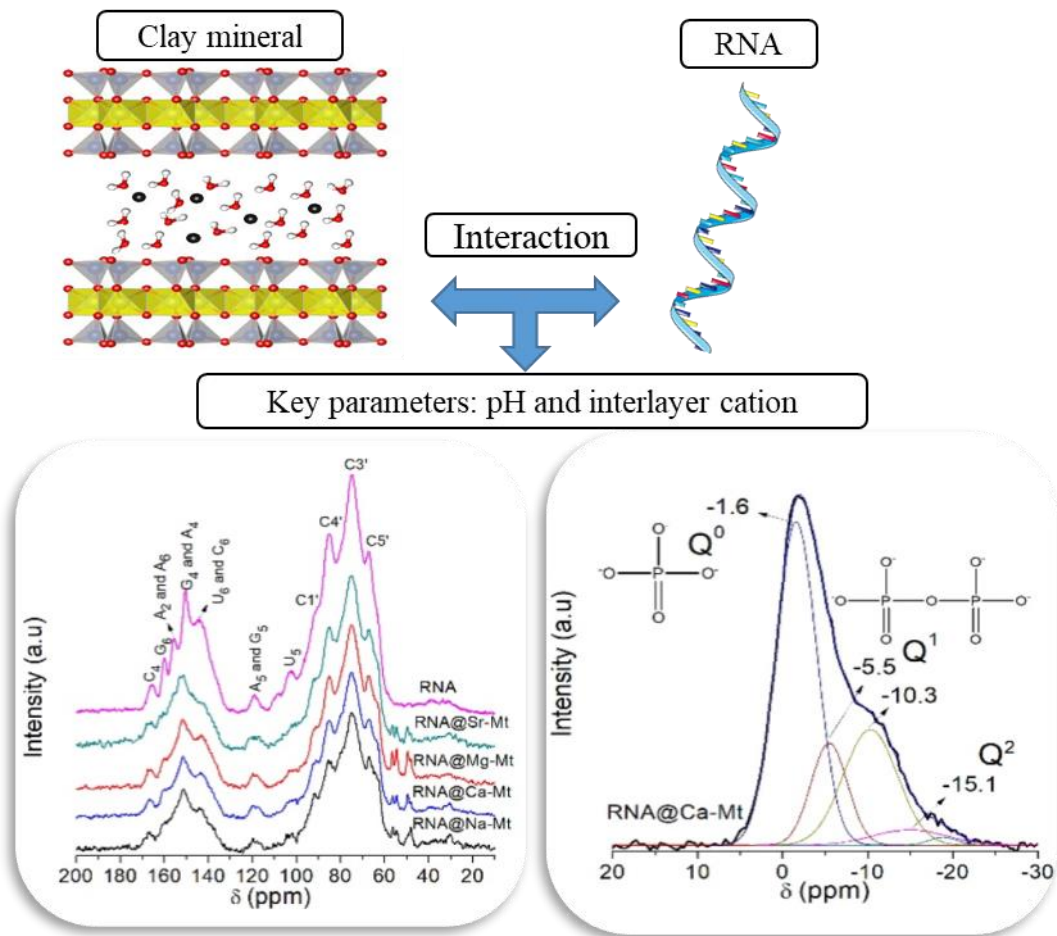
714 Wu, L., Liao, L., Lv, G., 2015. Influence of interlayer cations on organic intercalation of
715 montmorillonite. *J. Colloid Interface Sci.* 454, 1–7.
716 <https://doi.org/10.1016/j.jcis.2015.04.021>

717 Xie, H., Wan, Z., Liu, S., Zhang, Y., Tan, J., Yang, H., 2019. Charge-Dependent
718 Regulation in DNA Adsorption on 2D Clay Minerals. *Sci. Rep.* 9, 1–10.
719 <https://doi.org/10.1038/s41598-019-41093-5>

720 Yu, W.H., Li, N., Tong, D.S., Zhou, C.H., Lin, C.X., Xu, C.Y., 2013. Adsorption of
721 proteins and nucleic acids on clay minerals and their interactions: A review. *Appl.*
722 *Clay Sci.* 80–81, 443–452. <https://doi.org/10.1016/j.clay.2013.06.003>

723 Yukselen, Y., Erzin, Y., 2008. Artificial neural networks approach for zeta potential of
724 Montmorillonite in the presence of different cations. *Environ. Geol.* 54, 1059–
725 1066. <https://doi.org/10.1007/s00254-007-0872-x>

726



Full-size image:

